THE ASTROPHYSICAL JOURNAL, 294:533–545, 1985 July 15

THE KINEMATICAL AND PHYSICAL STRUCTURE OF HH 1 AND HH 2 DETERMINED FROM HIGH-RESOLUTION SPECTROSCOPY

K.-H. BÖHM[1,2] AND J. SOLF[2]

Received 1984 August 6; accepted 1985 January 28

ABSTRACT

Coudé spectra of high spatial and spectral resolution of the Herbig-Haro objects HH1 and HH2 and their environment have been used to study the spatial dependence of the radial velocity, the velocity dispersion, the electron density, and other properties. The observations, using a slit of 117″ length at different positions and position angles, contain a large amount of information not only about the structure of the HH objects but also about the physical conditions in their environment.

All our observations of HH 1 either agree with or at least do not contradict the expected radiation from a single bow shock due to a clump of gas moving almost perpendicular to the line of sight. The observations of HH 2 present more complex results. At present only part of them can be understood as the superposition of bow shocks due to independently moving clumps of matter. The space between the condensations seems to be filled with matter with electron densities N_e in the range 10^2–10^3 cm^{-3}. The observations often show "discontinuities" (drastic changes over a distance of $\sim 1''$) in N_e and the velocity dispersion at the "boundaries" of the condensations, whereas less steep gradients are found in the radial velocities. The discontinuities in N_e and the velocity dispersion are well correlated in a number of cases. The spatial variation of the radial velocity probably reflects small random changes in the direction of the velocity vectors of the individual clumps moving at high speed nearly perpendicular to the line of sight.

HH 1 and HH 2 are embedded in an environment showing faint line emission (at least) in Hβ, Hα, [N II] λλ6548, 6583, [S II] λλ6716, 6731, and [O III] 5007. Although these spectra are somewhat similar to that of the HH objects, they are probably not due to scattered light from these objects, since the [S II] line ratio indicates considerably lower density in the environment compared with the HH objects. We discuss the possible origin of the line emission from the environment.

Subject headings: nebulae: general — shock waves — stars: pre–main-sequence

I. INTRODUCTION

It is now generally accepted that the optical emission spectra of Herbig-Haro (HH) objects are found in the cooling (recombination) regions of shock waves (Schwartz 1975, 1978; see Schwartz 1983*b* and Böhm 1983 for recent reviews of this and related topics). On the other hand, not all observations of HH objects have been explained convincingly so far. For instance, the observed ultraviolet emission-line spectra (Ortolani and d'Odorico 1980; Böhm, Böhm-Vitense, and Brugel 1981; Brugel, Shull and Seab 1982; Böhm-Vitense *et al.* 1982; Schwartz 1983*a*) are not easily incorporated into the above interpretation (cf. Böhm 1983; Schwartz 1983*b*). Especially, the qualitative time changes recently found in the ultraviolet spectra (Brugel *et al.* 1985) may require considerably more sophisticated models, although we definitely believe that the basic idea of line formation in shock waves is correct.

Even more important for our present study is the fact that very little is known about the shape and the origin of the shock wave. It is fairly plausible to assume that the line spectra (and possibly the continua) of HH objects originate in a bow shock which may be formed either in the interaction of a strong stellar wind and a "cloudlet" ("shocked cloudlet model"; Schwartz 1978) or may be due to an "interstellar bullet" hitting some cloud material (Norman and Silk 1979). It may well be that more complicated models will be required. One such model has been introduced and investigated in considerable detail by Choe (1984).

In this paper we use spectra of high spatial and spectral resolution in order to determine the kinematical properties and the electron density as a function of position in two of these objects and their environment. Our hope is, of course, to derive from these properties information about the geometry of the shock (e.g., does it correspond to what is expected for the "interstellar bullet" model?). A preliminary interpretation of some of our observations (from HH 1) in terms of a "bow-shock model" has been surprisingly successful (Choe, Böhm, and Solf 1985). This investigation, however, made use of only a small fraction of our recently obtained high-resolution spectroscopic data. In this paper we present detailed empirical information derived for HH 1 and HH 2. The aim is to determine various maps (velocity, velocity dispersion, electron density) for the HH objects and their surroundings to be compared with model predictions. The main emphasis will be on the empirical results which can be deduced directly from our observations.

The first high-resolution spectroscopic studies of HH objects were due to Schwartz (1978, 1981) and Schwartz and Dopita (1980). These authors were concerned with the determination of (average) radial velocities and velocity dispersions for individual condensations. A very interesting study of line profiles at the positions of different condensations in HH 1 and HH 2 has been carried out by Hartmann and Raymond (1984). They, however, obtained one-dimensional spectra at a number of preselected positions (that is, centered on the known

[1] Astronomy Department, University of Washington, Seattle.
[2] Max-Planck-Institut für Astronomie, Heidelberg, FRG.

condensations). Hartmann and Raymond (1984) considered the spectrum formation in a bow shock in considerable detail. In these investigations, however, the authors did not study the details of the spatial variation of the emission-line spectra with high spatial resolution. Such studies are possible with a long-slit coudé spectrograph. We intend to show that a high-resolution determination of the variation of the emission-line spectrum inside HH objects and in their neighborhood leads to considerable new insight into the physics of these objects.

II. OBSERVATIONS

The observations were made during 1982 December with the vertical coudé spectrograph at the 2.2 m telescope of the Max-Planck-Institut für Astronomie at the Calar Alto Observatory, Spain. A two-stage magnetically focused image intensifier, cooled to $-18°C$, was used at the Newtonian focus of an f/3 camera of 90 cm focal length. The spectra were recorded on unbaked IIa-O photographic plates pressed onto the fiber optics output window of the tube. Using a 632 grooves mm^{-1} grating of 308×408 mm^2 ruled area in the second order, a reciprocal linear dispersion of 7.6 Å mm^{-1} was obtained on the spectrograms, covering a range of about 300 Å. Throughout the work the slit was set to a width of 2".2 and a length of 117" (projected onto the sky). The resulting spectral resolution is about 15 km s^{-1} (FWHM). The achieved spatial resolution on the long-slit spectrograms (mainly limited by the seeing) ranges from 1" to 2" (FWHM). In all cases the position angle of the entrance slit was set by means of an image derotator and was kept fixed during the exposure times of typically 30 min.

We have obtained four spectra of HH 1 and seven spectra of HH 2 at various slit positions and different spectral ranges. Detailed information about the observations is listed in Table 1. The slit positions are indicated in the photograph of the region in Figure 1 (Plate 5). The spectrograms were calibrated using a single-element Lyot filter according to the method described by Trefzger and Solf (1978). In order to remove the inherent geometrical distortion of the image tube, long-slit comparison spectra were recorded at various grating angles.

All spectrograms were raster-scanned on the PDS microdensitometer and reduced on the VAX computer of the Max-Planck-Institut in Heidelberg. An effective scanning aperture of 25×40 μm^2 (corresponding to 8.7 km s^{-1} in the direction of the dispersion and 1".1 in the direction of the slit) was used. The selected sampling intervals correspond to 1.7 km s^{-1} and 0".83, respectively. Details of the data reduction procedures have been described elsewhere (Solf and Carsenty 1982).

TABLE 1

JOURNAL OF OBSERVATIONS

Date 1982	Plate No.	Object	Slit Position[a]	Position Angle (degrees)	Spectral Range (Å)
Dec 15 .	S1250	HH 1	*a*	332	6480–6790
Dec 15 .	S1251	HH 2	*f*	45	6480–6790
Dec 15 .	S1252	HH 2	*e*	45	6480–6790
Dec 15 .	S1253	HH 2	*d*	45	6480–6790
Dec 15 .	S1254	HH 2	*g*	45	6480–6790
Dec 15 .	S1255	HH 2	*h*	45	6480–6790
Dec 15 .	S1256	HH 2	*c*	315	6480–6790
Dec 19 .	S1284	HH 1	*b*	62	6480–6790
Dec 19 .	S1285	HH 1	*a*	332	6140–6450
Dec 19 .	S1286	HH 1	*a*	332	4780–5090
Dec 19 .	S1287	HH 2	*c*	315	4780–5090

[a] See Fig. 1.

III. RESULTS

a) *Long-Slit Line Spectra*

In addition to the areas of the HH objects intersected by the particular slit positions, extended parts of the environment of the objects have been covered by the slit (see Fig. 1). Slit position *a* is centered on the Cohen-Schwartz (C-S) star (Cohen and Schwartz 1979; Mundt and Hartmann 1983) and goes through the brightest part of HH 1 (see Herbig and Jones 1981). The three spectrograms obtained at this position include the lines of Hβ, [O III] λλ4959, 5007, [O I] λλ6300, 6364, Hα, [N II] λλ6548, 6583, and [S II] λλ6716, 6731. The observed emission lines from position *a* are presented in Figure 2 (Plate 6) on enlarged portions of the spectrograms. The rather broad lines from HH 1 appear superposed on weak line emission from the environment. At this particular slit orientation we note that the "two-dimensional" line shape in HH 1 varies from line to line, resembling that of a triangle in most cases (e.g., Hβ) but being nearly circular in the case of [S II].

The narrow lines outside HH 1 are not appreciably affected by telluric emission lines except for [O I] and (to some small degree) Hα and [S II] λ6716. Near the center of the slit we note a weak continuum strip from the C-S star with a broad Hα emission feature. (Here and in the following illustrations, the top end of each spectrogram corresponds to that edge of the slit positions marked by the labels in Fig. 1.)

In addition, Figure 2 (*bottom*) displays the observed lines of Hα, [N II], and [S II] from slit position *b* perpendicular to the orientation of *a* and centered on the brightest part of HH 1. Although both slit orientations have the same (brightest) part of HH 1 in common, the two-dimensional line shape appears quite different in the two cases. Along the direction of slit position *b*, the line is quite symmetric and does not exhibit the triangular shape seen at slit position *a*. In contrast, the general properties of the line emission from the environment are the same in both slit positions.

The observations of the HH 2 field were also made at two slit position angles perpendicular to each other (see Fig. 1). At position *c* the slit crosses two of the brighter condensations, A and H, of HH 2 (see Herbig and Jones 1981; Herbig 1974) and points roughly in the direction of the C-S star. Portions of the spectrograms from this positions are reproduced in Figure 3 (Plate 7), displaying the lines of Hα, Hβ, [N II], [S II], [O III] and some weaker lines of [Fe II] and Fe III]. Comparing the various lines of the two condensations, we note interesting properties of the relative line widths (e.g., [O III] is broader in A than in H; the opposite is true for [S II]). The line emission from the environment of HH 2 does not seem to deviate from that of the HH 1 environment. The remaining slit positions, *d–h*, are covering most of the HH 2 region at 5" intervals (in right ascension).

In order to study the two-dimensional form of the emission lines of the long-slit spectra more quantitatively, from each line observed calibrated (logarithmic) intensity contour maps were prepared in a velocity (abscissa) versus angular position (ordinate) representation. The maps of various lines from HH 1 at slit position *a* are presented in Figure 4; those at position *b*, in Figure 5 (*top*). The maps of Hα, [N II] λ6583, and [S II] λ6731 from HH 2 at position *c* are shown in Figure 5 (*bottom*); those at positions *d*, *e*, *f*, and *g* are collected in Figure 6. Since

PLATE 5

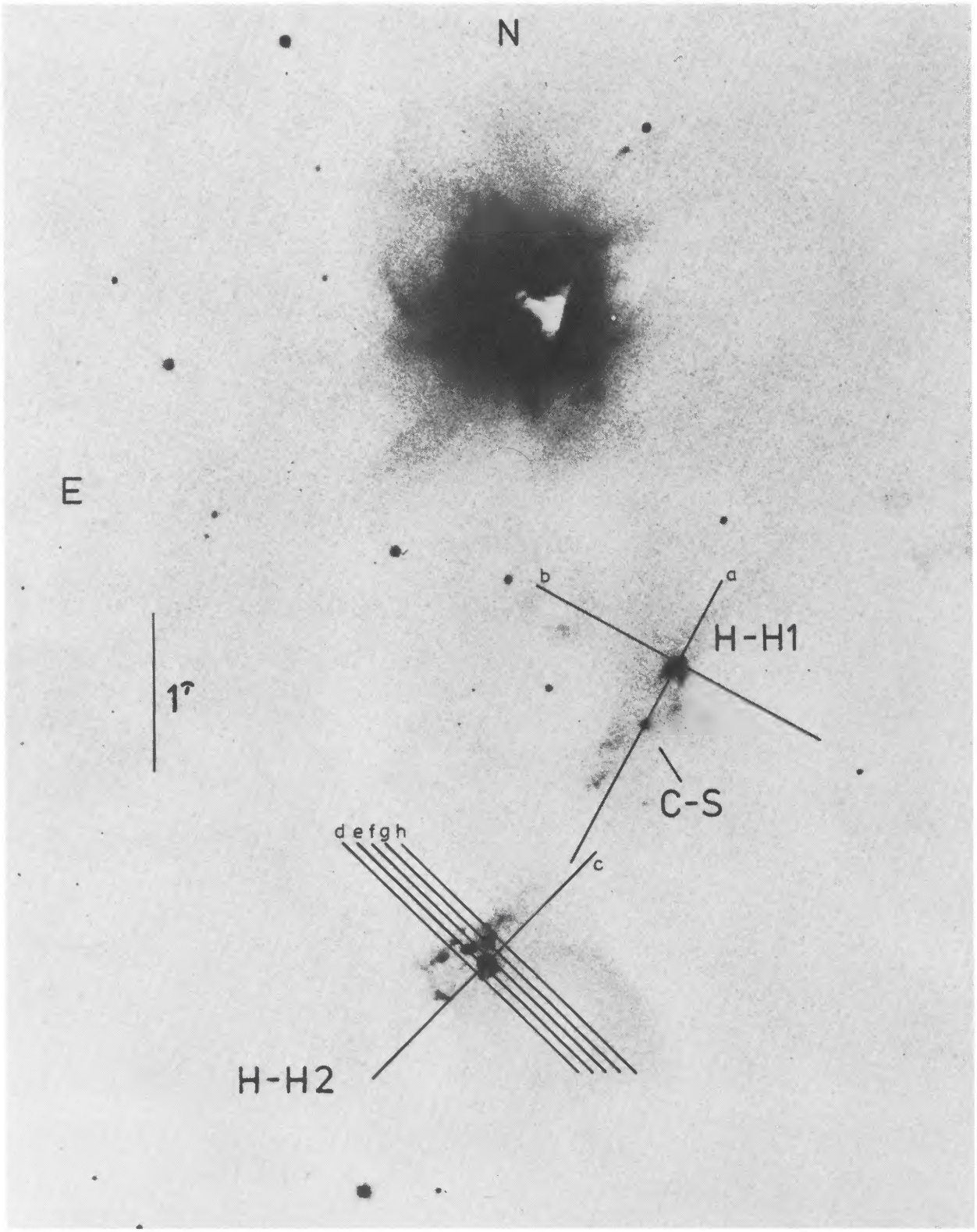

FIG. 1.—Region of HH 1 and HH 2. Photograph courtesy of Dr. G. H. Herbig. The positions of the spectrograph slit are shown and labeled from *a* to *h*. Slit position *a* is centered on the Cohen-Schwartz star (C-S) and covers the brightest parts of HH 1.

BÖHM AND SOLF (*see* page 534)

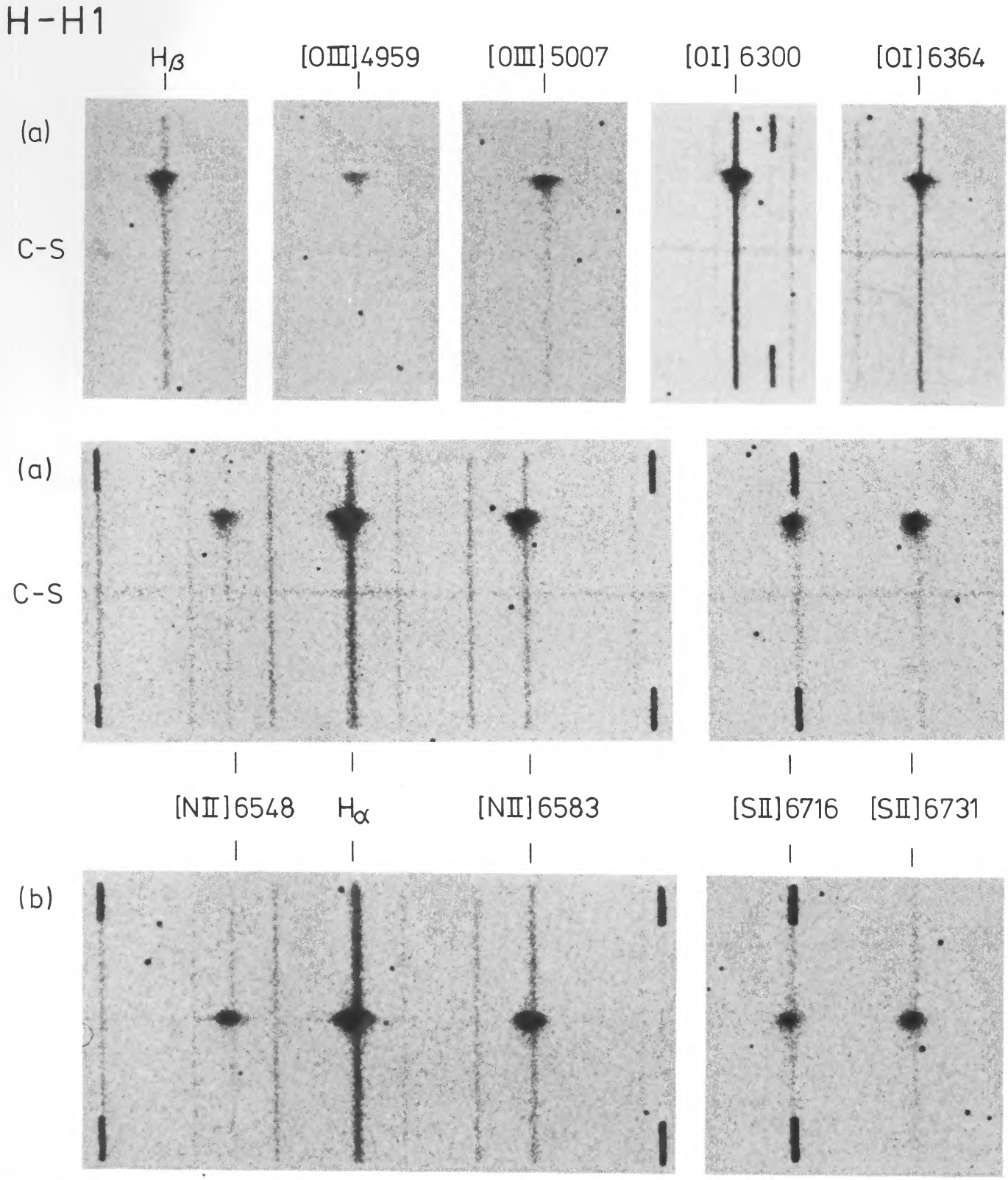

FIG. 2.—Enlarged portions of the long-slit coudé spectrograms of HH 1 and the interstellar environment observed at slit position *a* (*upper two rows*) and position *b* (*third row*). For slit positions see Fig. 1. The continuum spectrum from the C-S star is present at slit position *a*.

BÖHM AND SOLF (*see* page 534)

PLATE 7

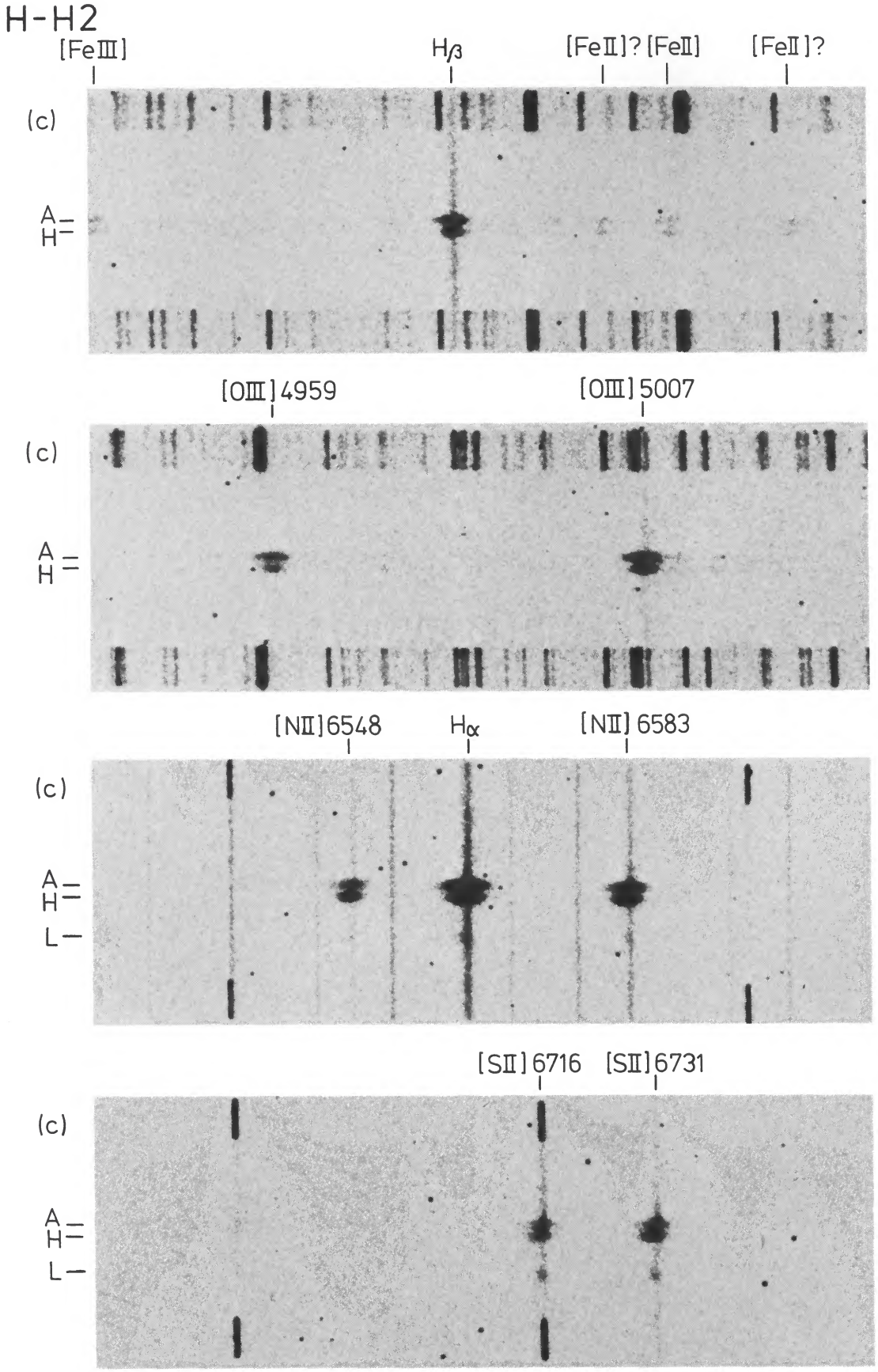

FIG. 3.—Enlarged portions of the spectrograms from HH 2 observed at slit position *c* (see Fig. 1). The relative positions of several condensations of HH 2 are marked in the left-hand margin.

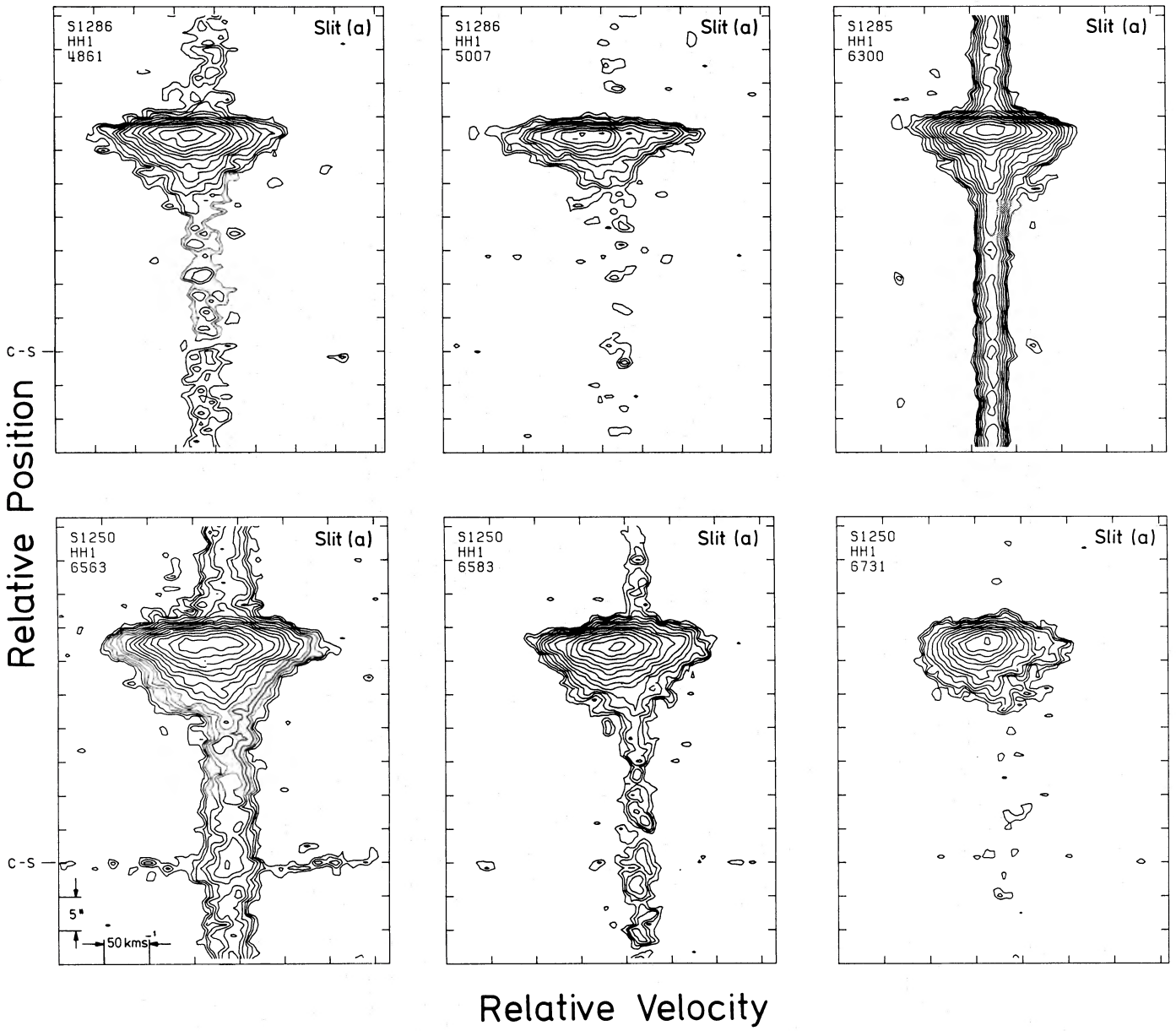

FIG. 4.—Intensity contour diagrams in a position versus velocity representation derived from various emission lines of HH 1 observed at slit position *a* (see Fig. 1). The contour intervals are logarithmic, each corresponding to a factor of $\sqrt{2}$. Plate number, object number, and line wavelength are stated in the upper left-hand corner of each diagram. Note the basically triangular shape of the contour lines in HH 1. Only the [S II] λ6731 line looks considerably different. The line radiation from the interstellar environment of HH 1 is visible, as well as some radiation (especially in Hα) from the C-S star (marked in the left-hand margin).

the emphasis of this paper will be on a study of the kinematics (derived from the line profiles) and the density distribution (using the [S II] λ6716/λ6731 line ratio) in and near HH 1 and HH 2, a comparison of spectrophotometric data at very different wavelengths is not required. Therefore, only the contour maps of Hα, [N II], and [S II] (for a particular slit position) use approximately the same intensity level (within 10%) for the first contour. Although the reddening and extinction are fairly well known for these objects (Böhm, Siegmund, and Schwartz 1976; Brugel, Böhm and Mannery 1981), an application of the reddening correction to our observations would not be useful in the context of this paper.

The contour maps reveal a rather complex spatio-kinematical structure of the HH objects, changing significantly over distances of a few arc seconds or less, most markedly shown in HH 2 (Fig. 6). At some positions, where the overall line width is well above 300 km s^{-1}, the line may represent two or more condensations which are spatially and kinematically unresolved.

b) Spatial Variation of Radial Velocity, Velocity Dispersion, and Electron Density

i) *General Remarks*

In order to obtain a better intuitive understanding of the objects HH 1 and HH 2, we have derived information about the local radial velocity, velocity dispersion, and electron density from our observations, using some representative slit positions, *a*, *b*, *c*, *e*, and *f*. The results have been plotted as a

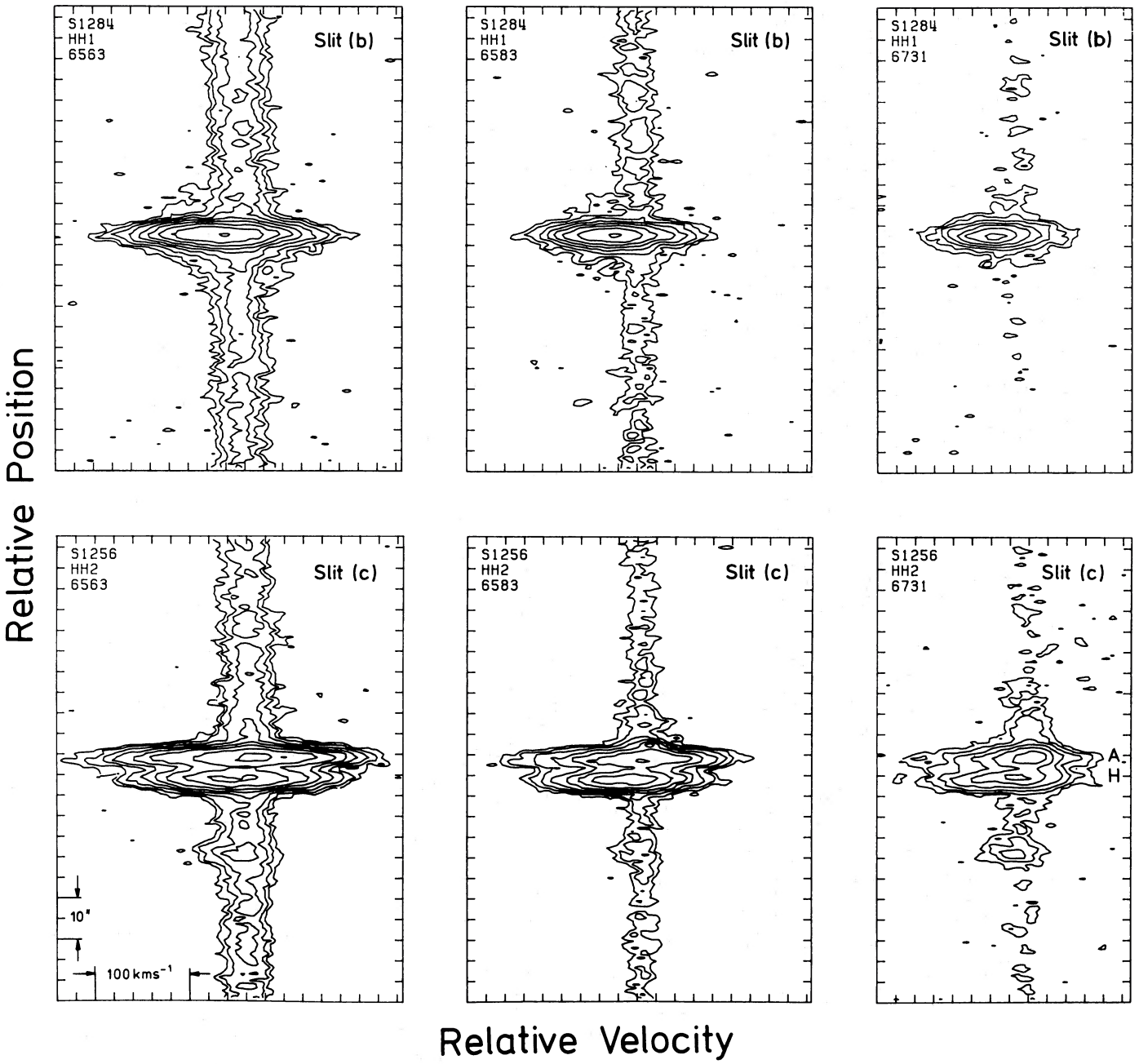

FIG. 5.—Intensity contour diagrams from Hα, [N II] λ6583, and [S II] λ6731 of HH 1 observed at slit position *b* (*upper row*) and of HH 2 observed at slit position *c* (*lower row*) (see Fig. 1). The contour spacings and the marking in the upper left-hand corners of the diagrams are analogous to those in Fig. 4. The relative positions of individual condensations of HH 2 are marked at the right-hand margin.

function of X, which designates the spatial position on the slit. $\Delta X = 1$ corresponds to 0".83 (used as the sampling interval on the PDS microdensitometer). Spectra have been measured at integer values of X in order to obtain the relative intensity, the "centroid radial velocity," the "half-width," and the "quarter-width" from the profiles of selected lines, and the electron density from the [S II] lines.

The intensity refers to the entire area under the local line profile, the centroid velocity to the center of gravity (with the area being equal on both sides of the measured wavelength). The half-widths and quarter-widths indicate the velocity spread at 50% and 25% intensity level, respectively, and have been measured to get an indication of the extended line "wings" which sometimes occur (see below). It is true that these velocity data represent only part of the kinematical information contained in the contour maps and do not reflect the fact that some of the individual condensations of the HH objects may not be sufficiently resolved in space. The partial overlap of the condensations seems to be indicated by line doubling or rather asymmetric profiles in a number of cases. We feel, however, that it is important to start out by considering first only some simple aspects of the results. The electron densities have been determined from the [S II] λ6716/λ6731 line ratio, using calculations of Koeppen (1983) based on the

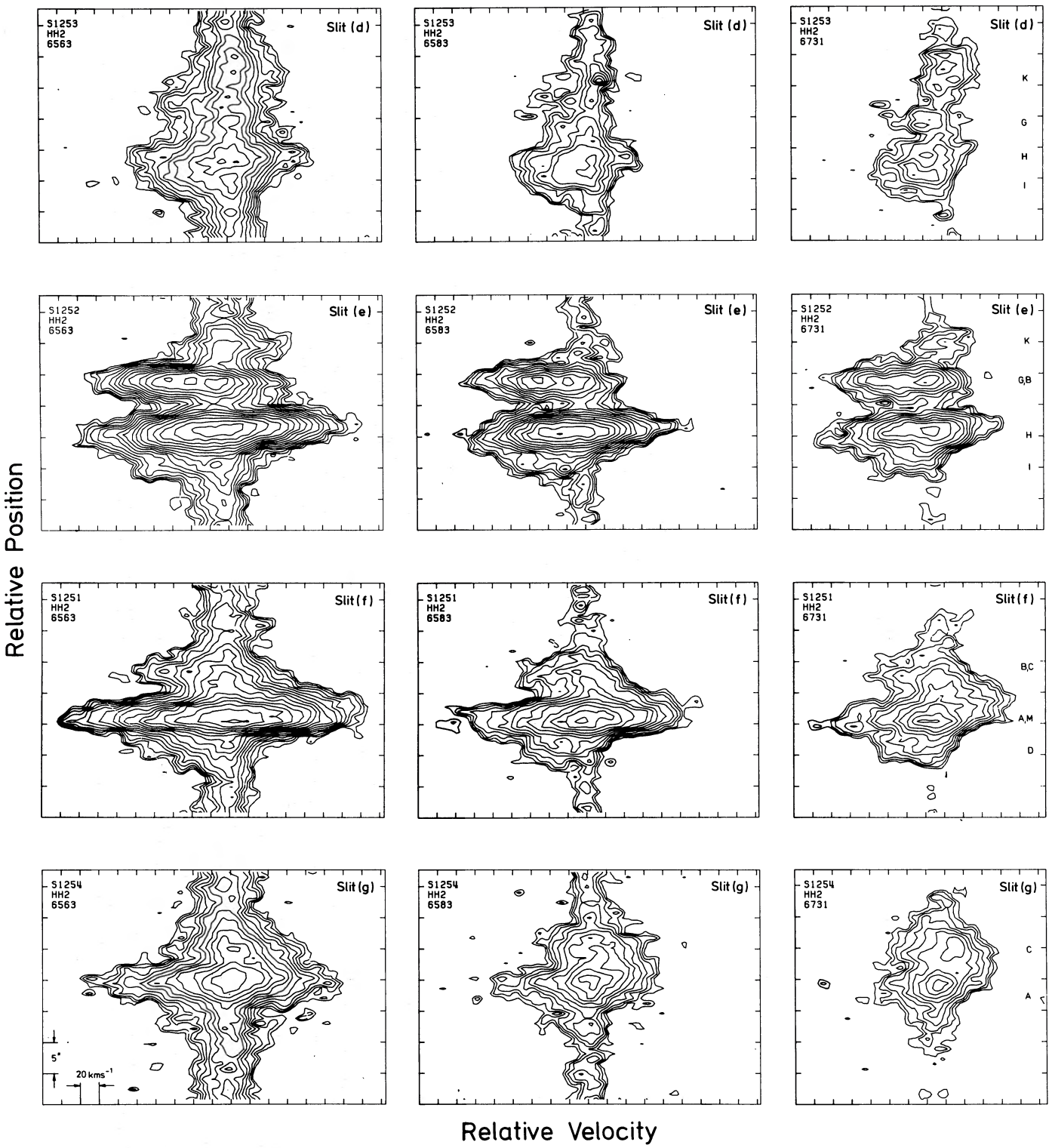

FIG. 6.—Intensity contour diagrams from Hα, [N II] λ6583, and [S II] λ6731 of HH 2 observed at slit positions *d*, *e*, *f*, and *g* (see Fig. 1) indicated in the upper right-hand corners of the diagrams. The other markings are analogous to those in Figs. 4 and 5.

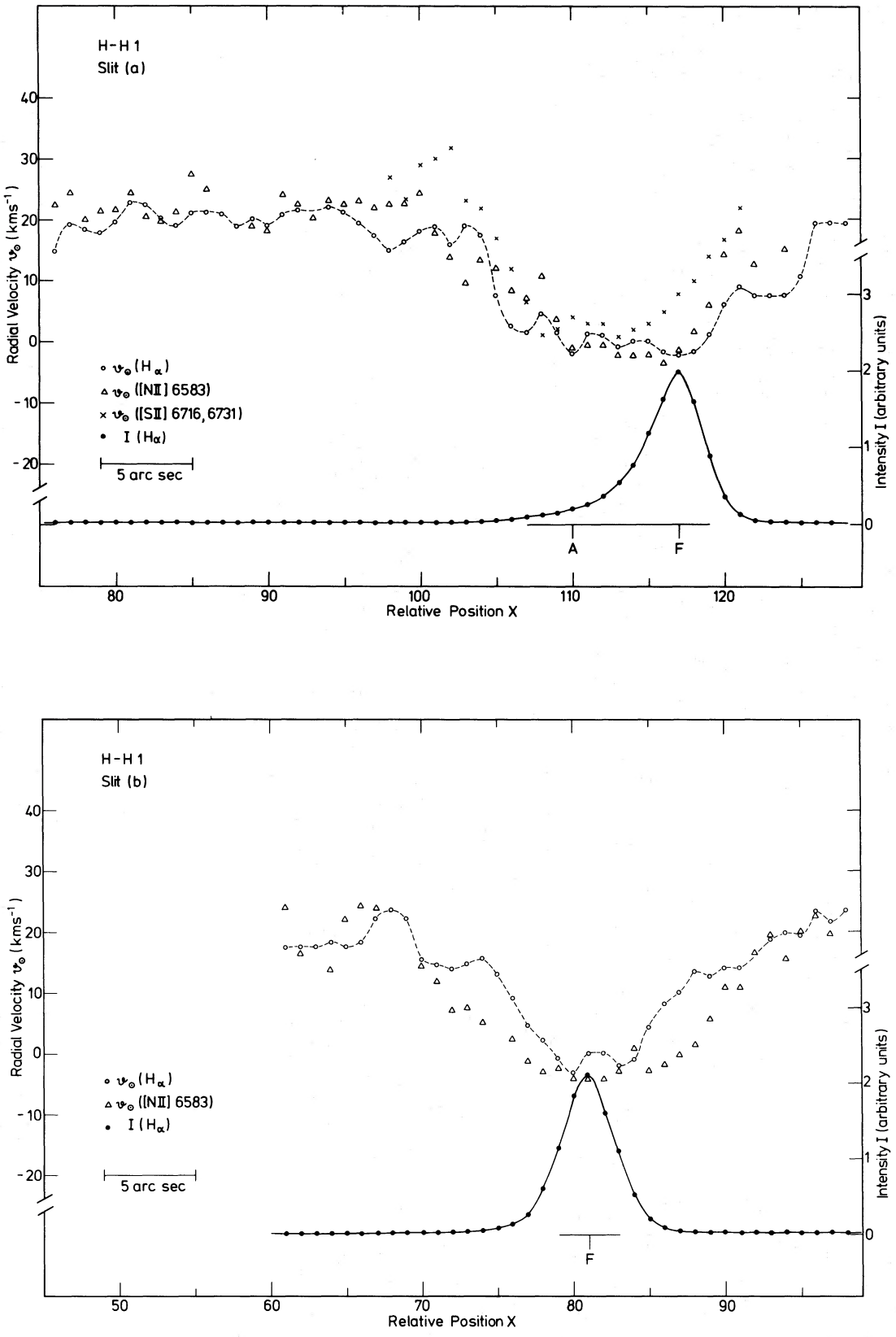

FIG. 7.—The centroid velocity as a function of the position coordinate X (with $\Delta X = 1$ corresponding to 0.″83; see text) for HH 1 and its environment, using slit positions *a* and *b* (see Fig. 1). The measurements have been made for the Hα and the [N II] λ6583 lines. In addition, mean values derived from the [S II] λλ6716 and 6731 lines are presented for slit position *a*. The spatial distribution of the Hα line intensity is also shown.

collision line strengths given by Pradhan (1978). (Generally a 3-point smoothing has been applied to the electron density data.)

Every measurement has been made in the spatial range in which the line intensities were sufficiently strong. Consequently, the spatial coverage is somewhat different for the determination of different physical quantities. Furthermore, it is well known that a reliable determination of N_e from the [S II] line ratio above, say, $N_e \sim 1 \times 10^4$ cm^{-3} or below $N_e \sim 100$ cm^{-3} requires very accurate spectrophotometric data. (See Osterbrock 1974.) Since our data are based on photographic material, the detailed shape of the density curves outside this range is not well known.

ii) *HH 1*

In Figure 7 we present the spatial variation of the line intensity (Hα) and the (centroid) radial velocities from Hα and [N II] λ6583 for the two slit positions *a* and *b* going through the brightest part of HH 1. For a limited extent within the slit position *a* the radial velocity from the [S II] lines (average values from [S II] λλ6716 and 6731) is shown as well. It should be noted that slit position *a* (crossing the C-S star) has been aligned nearly parallel to the mean direction of the high proper motion of HH 1 discovered by Herbig and Jones (1981). (The direction of the proper motion is toward higher X-values in our diagram of Fig. 7.) The slit orientation *b* is perpendicular to the proper motion.

As can be seen from Figure 7, the spatial variation of the radial velocity resembles a "trough," i.e., the velocity within HH 1 is negative with respect to the constant velocity of the environment. In the case of slit position *b* the through is rather symmetric and centered near the maximum of the line emission. (The spatial extent of this trough seems to be somewhat larger for the [N II] velocities compared with those of Hα.) In the case of slit position *a* the velocity data are much less correlated with the intensity distribution. The trough in the velocity distribution is considerably broader than in the case of position *b*. Only near the "front edge" of the moving HH 1 object ($117 \leq X \leq 120$) does the drop in the velocity coincide with the steep rise in the intensity. On the "backside" of HH 1 ($X < 117$) the low velocity continues at a nearly constant value to a spatial position where the intensity has dropped well below 5% of the maximum. Generally, the velocities derived from [N II] and [S II] are in reasonable agreement with the Hα data.

Figure 8 shows (*from top to bottom*) the spatial variations of the half-width $\Delta v_{1/2}$, the quarter-width $\Delta v_{1/4}$, and the electron density. Because of the difficulties (mentioned above) in deducing electron densities above $N_e \sim 10^4$ cm^{-3}, we have artificially limited the maximum of N_e to 2×10^4 cm^{-3}. Consequently any point with $N_e = 2 \times 10^4$ cm^{-3} *may* in reality have a higher electron density than is shown. It is useful to realize that in spite of the applied 3-point smoothing of the N_e data (see above), very large gradients in the density distribution occur, e.g., near the "front edge" of HH 1 ($X \sim 122$), where N_e increases by about a factor of 10 with a distance of about 1″.

iii) *HH 2*

For this object we have restricted this evaluation to only a few of the observed slit positions. The spatial distributions of the (relative) intensity and of the centroid radial velocity for positions *c*, *e*, and *f* are presented in Figure 9. Generally, the velocity data from Hα and [N II] are in reasonable agreement.

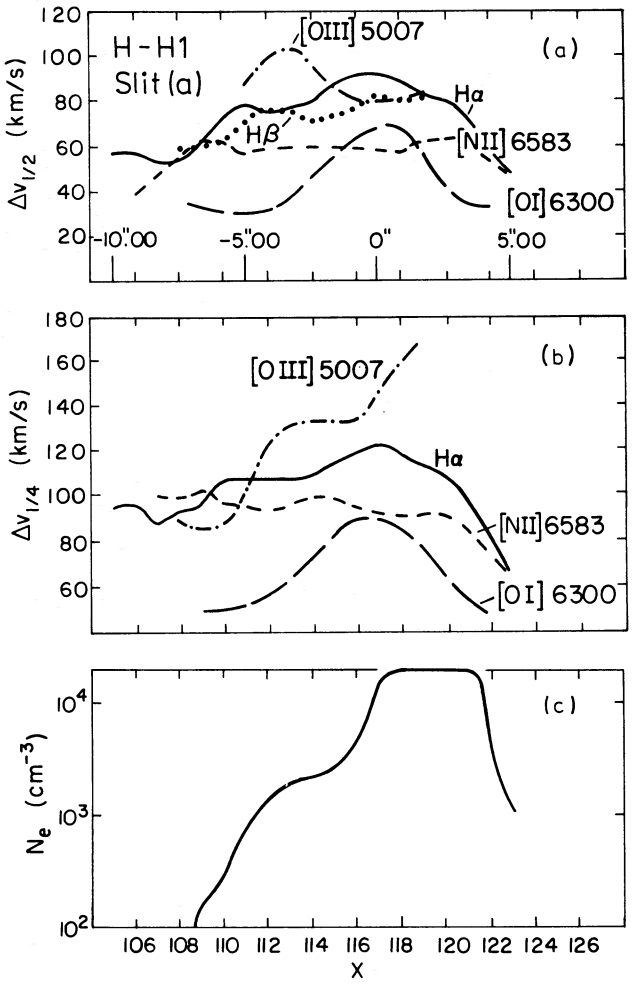

FIG. 8.—(*a*) The half-width $\Delta v_{1/2}$, (*b*) the quarter-width $\Delta v_{1/4}$, and (*c*) the electron density N_e (determined from the [S II] λ6716/λ6731 ratio) as a function of the position coordinate X in and near HH 1 for slit position *a* (see Fig. 1). Note the steep increase of N_e at the northwest edge of HH 1 ($X \sim 122$) and the correlated increase of $\Delta v_{1/2}$ and $\Delta v_{1/4}$ for most lines. Of special interest is also the presence of extended wings (indicated by the large value of $\Delta v_{1/4}$ between $X = 117$ and $X = 119$) in the [O III] λ5007 line in a limited region.

On the other hand, the spatial variation of the velocity is not well correlated with the intensity distribution in a number of cases. We note that different condensations (of various brightness) may show different mean radial velocities, but it is obvious that some condensations (e.g., A or H) exhibit large velocity gradients near their intensity maximum. These findings suggest that some of the condensations of HH 2 may consists of spatially unresolved subcomponents which have different radial velocity components and are likely to be distinct along the direction of the line of sight.

In Figure 10 we present the velocity dispersions $\Delta v_{1/2}$ and $\Delta v_{1/4}$ as well as the electron densities N_e along slit position *e*. In contrast to the radial velocities (Fig. 9), the distributions of $\Delta v_{1/2}$, $\Delta v_{1/4}$, and N_e are well correlated with the positions (intensity maxima) of the individual condensations. The velocity dispersions and electron densities along slit position *c* are shown in Figure 11. Again, the condensation structure can be recognized well in the diagrams. This is especially true for the N_e diagram, where large density gradients occur near the "edges" of the condensations.

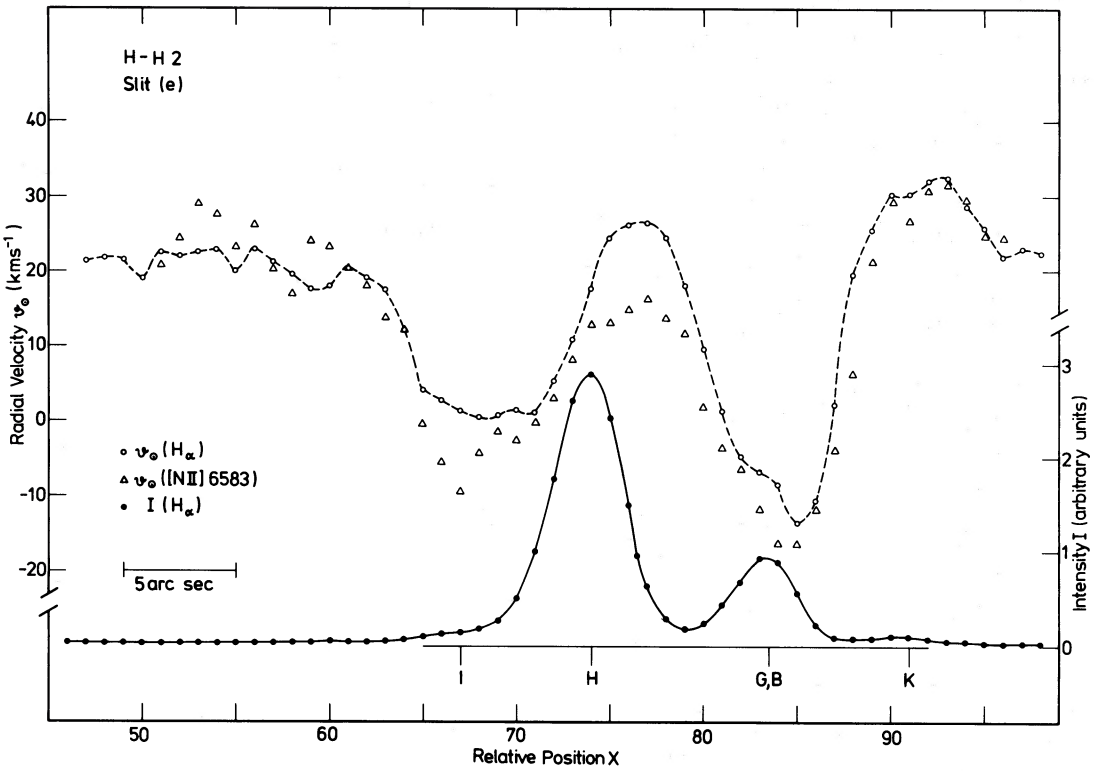

FIG. 9*a*

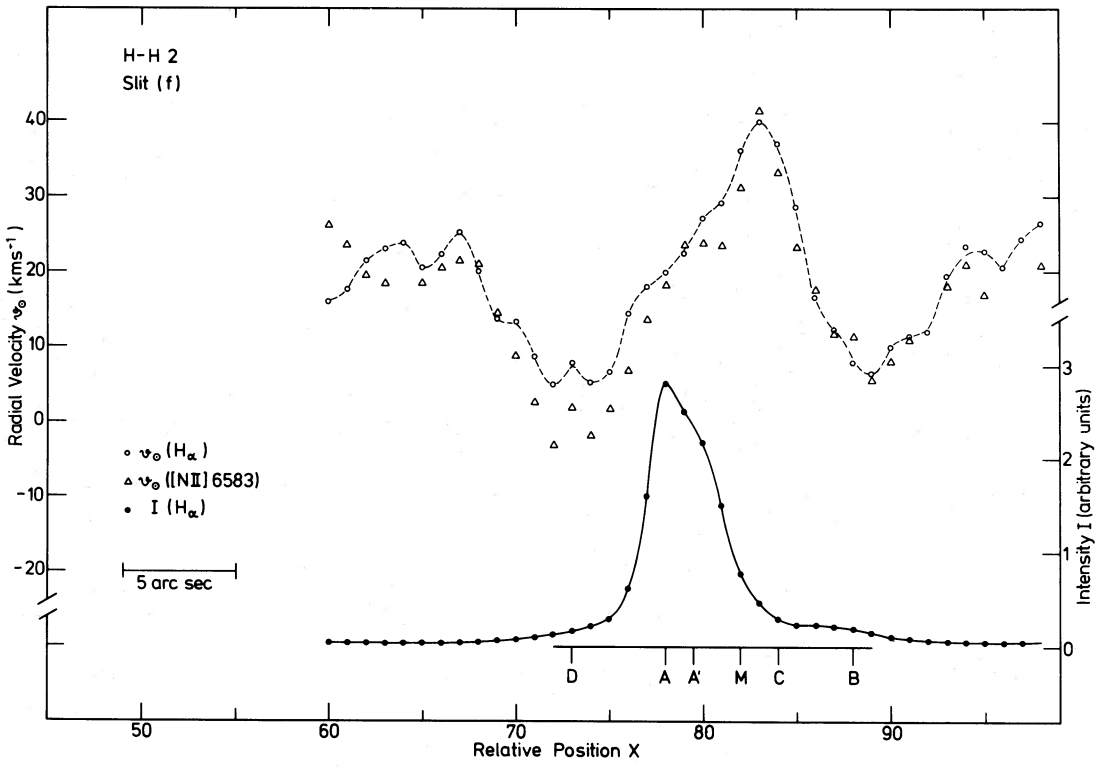

FIG. 9*b*

FIG. 9.—The centroid velocity as a function of X (see Fig. 7) for HH 2 and its environment deduced from slit positions *e* (Fig. 9*a*) and *f* (Fig. 9*b*) (see Fig. 1) indicated in the upper left-hand corners. The spatial distribution of the Hα line intensities is also shown.

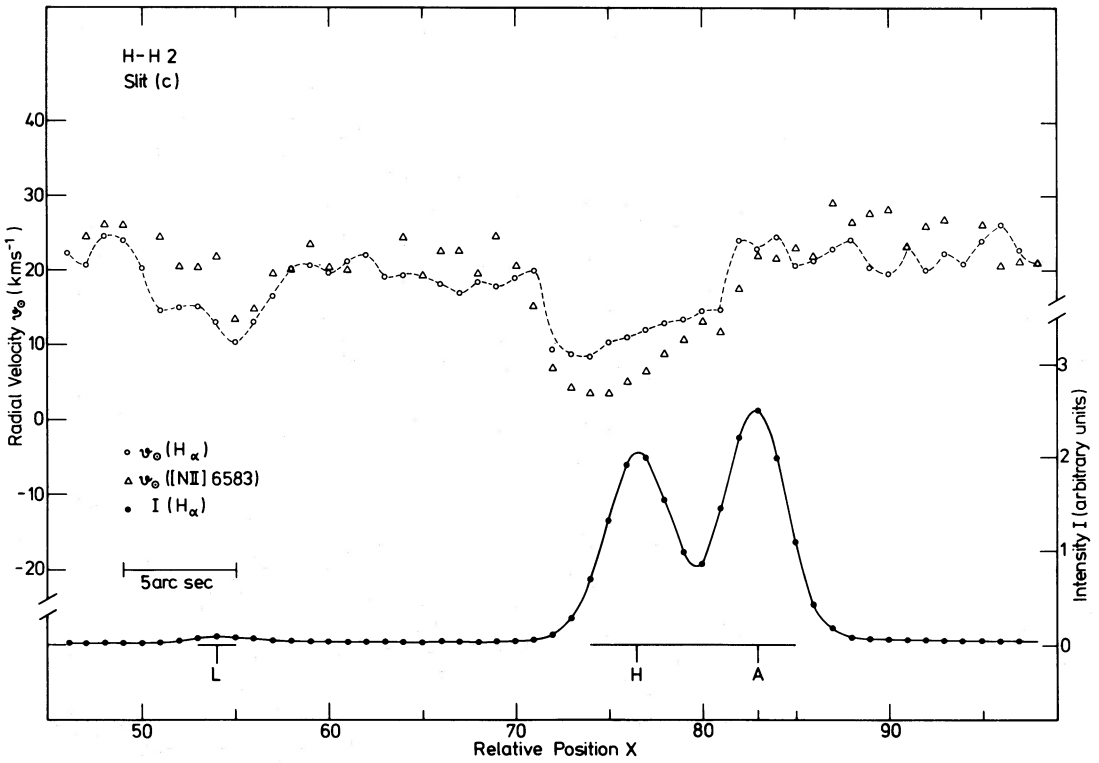

FIG. 9c.—Same quantities as in Figs. 9a and 9b deduced from slit position c

iv) *The Environment of HH 1 and HH 2*

The use of long-slit spectra enables us to deduce physical parameters not only for the HH objects themselves but also for their environment. We have observed line emission from Hβ, Hα, [O III], [N II], and [S II] over the full length of the slit (117″) at each slit position. ([O I] is masked by the atmospheric lines.)

As can be seen in Figures 2 and 3, the environment lines of [N II] and [S II] are of considerable strength relative to Hα. On the other hand, [O III] λ5007 is markedly weaker than Hβ. These relative line intensities are more typical for HH objects than for "normal" H II regions. The line strengths change only slightly (~30%) with the position on the slit (the regions immediately around the HH objects are not considered). In Table 2 we list the mean values for the radial velocities, line widths, and relative line strengths obtained from the environment lines of Hα, [N II] λ6583, and [S II] λλ6716, 6731. These main values represent averages from several slit positions and were deduced from spatial intervals corresponding to a few arc minutes. The line ratios [N II]/Hα and [S II]/Hα in the environment (estimated error less than 50%) are smaller only by a factor of 2 or so than the corresponding line ratios observed in HH 1 and HH 2 (Brugel, Böhm, and Mannery 1981; Hartmann and Raymond 1984). The [S II] λ6716/λ6731 ratio quoted in Table 2 (estimated error less than 20%) has been corrected for a small contamination in the [S II] λ6716 line (10%–20%) from the night sky.

IV. DISCUSSION

a) General Remarks

One of the outstanding features of our results is the relatively frequent occurrence of very steep spatial gradients in the electron density, the line intensity (which is, of course, not independent of N_e), and the velocity dispersion. In a number of cases the gradients are so steep that they are compatible with the assumption of discontinuities which are slightly broadened by seeing effects. The reality of these steep gradients is shown by the fact that steep increases in the velocity dispersions in different lines and steep increases in the electron density are usually well correlated with each other. The discontinuous character of the velocity dispersion is also indicated by the contour diagrams. The behavior of the line profiles at the northwest edge of HH 1 (Fig. 4) is a good example (though of course one has to distinguish increasing velocity dispersion from increasing line intensity.) We shall now discuss some interesting properties of HH 1 and HH 2 separately.

b) HH 1

The contour diagrams of HH 1 are especially interesting. For a slit orientation along the connecting line between HH 1 and the C-S star (position angle −28°) we present contour diagrams ("position-velocity" diagrams) (Fig. 4) in which all

TABLE 2

ENVIRONMENT OF HH 1 AND HH 2

Parameter	Hα	[N II] λ6583	[S II] λλ6716, 6731[a]
Radial velocity $v_\odot$ (km s^{-1})	20.8	23.7	...
Line width (FWHM) (km s^{-1})	34	21	...
Line strength (relative to Hα)	1	0.20–0.25	0.20–0.25

[a] Line ratio [S II] λ6716/λ6731: 1.36.

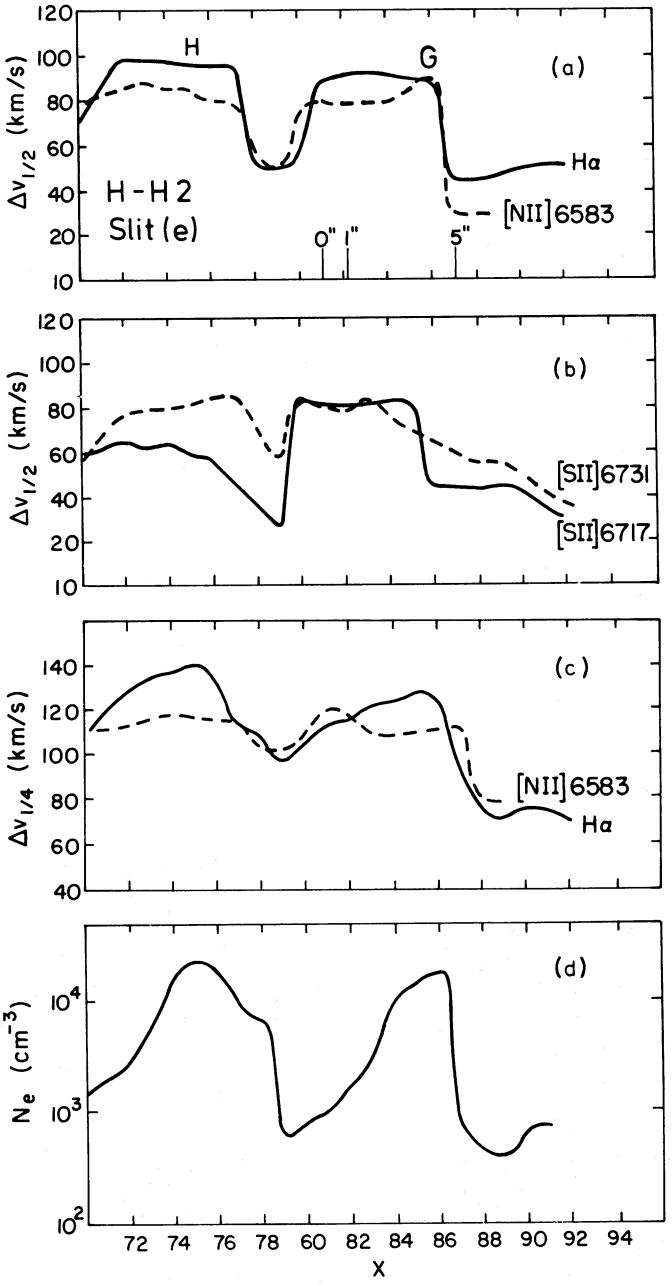

FIG. 10.—The half-width $\Delta v_{1/2}$ (*a*) for Hα and [N II] λ6583, and (*b*) for [S II] λλ6731 and 6716; (*c*) the quarter-width $\Delta v_{1/4}$ for Hα and [N II] λ6583; and (*d*) the electron density N_e as a function of X. The diagrams refer to slit position *e* for HH 2 (see Fig. 1).

lines, except [S II] λλ6716, 6731, show a triangular shape inside the HH object with the horizontal side on top. It has been shown by Choe, Böhm, and Solf (1985) and Raga and Böhm (1985) that such a shape is (at least qualitatively) to be expected if we see the bow shock of an approximately spherical object which moves away from the C-S star perpendicular to the line of sight into a medium which is approximately at rest relative to the C-S star. It follows from the large proper motions of individual knots (corresponding to up to 350 km s^{-1}; see Herbig and Jones 1981) and the small radial velocities (~20 km s^{-1} and less; see below) that the motion of HH 1 and HH 2 is indeed essentially perpendicular to the line of sight.

We shall now discuss the interpretation of the HH 1 results in terms of the radiation of a bow shock generated by a spherical "bullet" (Norman and Silk 1979) moving perpendicular to the line of sight into a medium at rest with respect to the C-S star. We find it surprising how well the observations agree qualitatively with the predictions of such a model.

Although the theoretical explanation of the "triangular shape" of the emission-line contour diagrams is derived and discussed in the papers by Choe, Böhm, and Solf (1985) and Raga and Böhm (1985) in detail. We shall present here a *brief* qualitative description. We assume that a spherical "bullet" moves away from the star perpendicular to the line of sight, with high Mach number. (See the numbers quoted in the first paragraph of this subsection.) In such a situation the flow near the front side of the ("blunt") bullet (i.e., near the stagnation point) has essentially the same direction as the surface of the "bullet," i.e., there is a strong velocity component perpendicu-

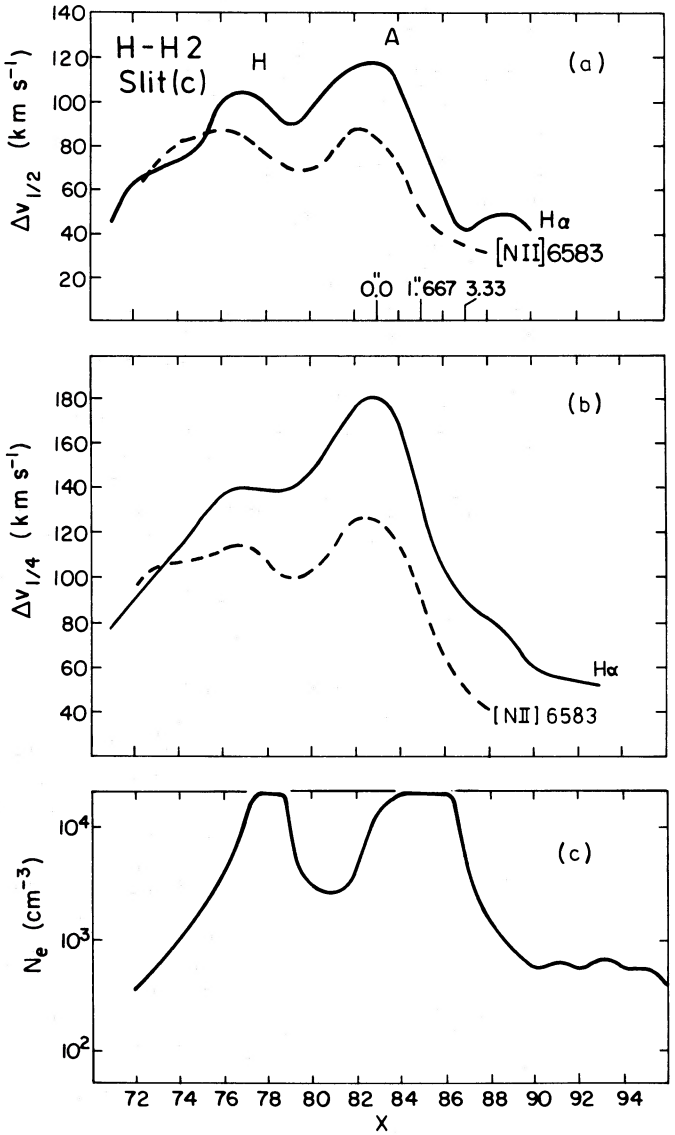

FIG. 11.—(*a*) The half-width $\Delta v_{1/2}$, (*b*) the quarter-width $\Delta v_{1/4}$, and (*c*) the electron density N_e as a function of X for slit position *c* in object HH 2 (see Fig. 1).

lar to the main flow. In other words, while the motion of the "bullet" is perpendicular to the line of sight there will be strong radial velocity components near the stagnation point. But the flow is of course symmetric around the axis of the bow shock, which is perpendicular to the line of sight. Consequently we do not get a shift but a broadening of the line near the stagnation point. In a flow of high Mach number the bow shock occurs very close to the front side of the bullet, i.e., the line broadening starts very abruptly. This sudden onset of large radial velocity dispersions corresponds to the horizontal edge in our diagrams (cf. Fig. 4). As we follow the bow shock around the "bullet," the flow becomes more and more parallel to the axis of the bow shock (which is perpendicular to the line of sight), the radial velocity dispersion declines, and the line becomes narrower (the lower part of the triangle; see Fig. 4). All these facts have been demonstrated quantitatively in the papers quoted above.

Other aspects of the theoretical predictions which seem to be confirmed by our present observations of HH 1 include the following. Under conditions which are approximately fulfilled for Herbig-Haro objects, the bow shock can be approximated by small pieces of plane oblique shocks for the purpose of calculating its line emission. (Hartmann and Raymond 1984; Choe, Böhm, and Solf 1985; Raga and Böhm 1985). For a given bow shock we find that the greatest shock strength occurs at the stagnation point. The shock strength declines toward the "tail" of the bow shock because the shock becomes more oblique and the (normal) velocity jump becomes correspondingly smaller. This has the consequence that high-ionization lines such as, e.g., [O III] λ5007 which require relatively strong shocks can be formed only in a relatively small region near the stagnation point. Consequently the triangle in the contour diagram for this line will be shallower than, for example, those for the [N II], [O I], and the Balmer lines. This conclusion is again confirmed by detailed calculations (Raga and Böhm 1985).

From these arguments (and in agreement with the quoted calculations) it is clear that for a "bullet" moving away from the star (in this case the C-S star) we should in the contour maps for all lines see a triangular shape with the horizontal side on the far side from the star. In the shocked cloudlet model (Schwartz 1978) the stagnation point of the bow shock would be on the side toward the star and the triangle should be inverted, with the horizontal side on the side toward the star.

Using this information, we can conclude the following from the observed contour maps of HH 1 which are presented in Figure 4. All contour diagrams (with the possible exception of the one for [S II] λ6731) are, at least qualitatively, compatible with the predictions for the bow shock around a "bullet" coming from the direction of the C-S star and moving into a medium which is essentially at rest with respect to the star. The fact that the [O III] λ5007 contours form a much shallower triangle is also predicted by this model. (A quantitative comparison of the predicted and observed Hβ contour map has been given by Choe, Böhm, and Solf 1985.) Finally, the fact that the triangular shape is replaced by a flat symmetric shape in the contour maps for slit orientation *b* (see Fig. 5) is also in agreement with the predictions of the bow shock theory. Only the behavior of the [S II] $\lambda\lambda$6716, 6731 lines is not well understood. These lines do not show so pronounced a triangular shape as the other lines. On the other hand, as expected, the bow shock theory predicts (Raga and Böhm 1985) that the [S II] λ6731 and the [N II] λ6583 contour lines should look very similar. This discrepancy is not yet understood. In fact, it is not easy to see how any theory could lead to essentially different contour maps for the [S II] and [N II] lines.

The conclusions drawn from the study of the contour diagrams are in part confirmed by the study of the spatial variation of the electron density, the velocity dispersion (Fig. 8), and (to a lesser extent) the radial velocity (see Fig. 7). A clear "discontinuity" (i.e., a very steep gradient) in N_e occurs at the northwest edge of HH 1 between $X = 123$ and $X = 122$ (Fig. 8*c*). We tentatively identify this region with the environment of the stagnation point of the bow shock. This region also shows a fairly steep increase in the half-width and quarter-width especially of Hα and of [N II] λ6583 (Figs. 8*a* and 8*b*).

It is interesting that the decline of the velocity dispersion behind the HH object is much slower than the decline of N_e and that of the Hα intensity. In fact, with the exception of the [O I] λ6300 line, the velocity dispersion $\Delta v_{1/4}$ does not return to its original value within the range of X-values in which $\Delta v_{1/4}$ can be measured in individual spectra. This is again qualitatively in agreement with the theoretical prediction for a bow shock seen "side-on" in which the shock ionization disappears rather rapidly at a certain distance behind the "bullet" but the measurable velocity dispersion does not decline rapidly (Raga and Böhm 1985). The reason for this effect is again (analogous to the above discussion of the [O III] λ5007 line) that in the downstream parts of the bow shock the shock becomes weak. This has the consequence that the ionization (including that of hydrogen) drops drastically. Consequently the electron density and the emission coefficient become smaller much faster than the velocity field itself. The rapidly rising width of the line wings of [O III] λ5007 from $X \sim 116$ toward $X \sim 118$ (as measured by the "quarter-width"; see Fig. 8*b*) may also be compatible with bow shock predictions, but we are not yet in a position to prove this.

In general, we find that there is a considerable number of indications that HH 1 is a bow shock directed away from the C-S star as in the interstellar bullet model (Norman and Silk 1979). It is surprising that most of the observational results seem to point in this direction or, at least, do not seem to contradict this explanation, although HH 1 consists of individual condensations having individual proper motions (Herbig and Jones 1981).

We do not have any good explanation for this fact. It is not yet clear whether a scenario would be possible in which the condensations occur inside an overall flow pattern corresponding to a single bow shock. On the other hand, it would be surprising indeed if the different points of agreement between HH 1 observations and bow-shock theory were all accidental.

c) HH 2

The physical conditions are much more complex in HH 2. Looking at the complex structure of the contour diagrams (Figs. 5 and 6), it is not surprising that the interpretation of the line profiles appears quite difficult in this case. From the figures it seems obvious that every "condensation" has its own velocity field, with velocity dispersion and density going down to relatively low values between the condensations.

It would be very difficult to investigate a detailed gas-dynamic model for HH 2 which would have to include, for example, the nonlinear interactions between a number of different bow shocks. We shall therefore restrict ourselves to more general conclusions which can be derived directly from our observations. We should mention, however, a bold attempt

by Choe (1984), who has tried to explain our position-velocity map going through condensations A and H (Fig. 5) as being due to two independently moving "bullets."

Let us now look at the more general conclusions which we can draw from our results. These spectra again show the fact that the Herbig-Haro phenomenon is a consequence of hydrodynamic processes: The brighter condensations (such as HH 2 H, HH 2 G, and HH 2 A) show a much greater velocity dispersion than the fainter condensations and the regions between condensations. (See especially Fig. 6.)

If we look at N_e (Figs. 10 and 11), it is worth noting that two neighboring condensations typically have the N_e "discontinuities" pointing in the same direction for both condensations. It is also impressive that often discontinuities in N_e and in the velocity dispersion occur at the same position to a high degree of accuracy ($\sim 1''$).

Another interesting result is the complexity of the appearance of N_e discontinuities and the fact that the most pronounced discontinuity sometimes seems to appear at an angle of 90° to the one which we expect from the proper-motion observation. Figure 11*c*, for example, shows that the largest N_e gradient occurs at $X = 79$ (HH 2 H) and $X = 87$ (HH 2 A) and appears on the side *toward* the C-S star in both cases (contrary to the results for HH 1). Even larger gradients occur, however, for a position angle almost perpendicular to the connecting line with the C-S star (Fig. 10*c*, going through condensations G and H). The discontinuities now occur on the northeast side of the condensations. It is tempting to speculate whether the faint infrared source seen by Cohen and Schwartz (1979) directly east of HH 2 may have anything to do with this behavior.

In summary, we conclude that because of its complexity HH 2 cannot be explained by a fairly simple bow shock model as seems to be the case for HH 1. On the other hand, there seem to be obvious analogies between HH 1 and HH 2, e.g., with regard to the appearance of discontinuities in N_e and in the velocity dispersion. It is reasonable to assume that in HH 2 we see the interaction of a number of bow shocks.

d) The Environment of HH 1 and HH 2

One interesting aspect of our observations is the possibility of studying the emission lines formed in the environment of HH objects. The environment of both HH 1 and HH 2 radiates in most of the lines which are typical for HH objects, although the line ratios are not the same as in the HH objects. Hβ, Hα, [N II] $\lambda\lambda$6548, 6583, and [S II] $\lambda\lambda$6716, 6731 are detectable, though of course much fainter than in the objects themselves. Although these lines have been seen on spectra obtained by other authors, they have not yet been studied quantitatively.

Even if the line ratios in the environment deduced from our observations are of only moderate spectrophotometric accuracy (see above), we can draw interesting (and unexpected) conclusions from our results. In the environment of HH 1 and HH 2 the ratio [S II] λ6716/λ6731 shows a value which is close to the low-density limit (see Table 2). If we interpret the measured value for the spatial average of the ratio λ6716/λ6731, we find an electron density of ~ 100 cm^{-3} (using Koeppen's 1983 results). This value is very different from that of HH 1 and the brighter condensations of HH 2 in which the ratio [S II] λ6716/λ6731 is always fairly close to its high-density limit. This fact clearly shows that the faint emission-line spectra seen in the environment of HH 1 and HH 2 are *not* due to scattered light coming originally from the HH objects themselves. Could it be scattered light coming originally from the Orion Nebula (or another H II region in the Orion complex)? This is excluded by the fact that both the [S II] λ6716/λ6731 and the [S II] (λ6716 + λ6731)/Hα line ratios in the environment of HH 1 and HH 2 do not agree with typical line ratios in the Orion Nebula (cf. Goudis 1982), where high electron densities prevail and the [S II]/Hα line ratio amounts to only a few percent instead 20%–25% (Table 2).

It seems to us that the most straightforward conclusions which can be drawn are the following. The environment of HH 1 and HH 2 emits an emission-line spectrum. This is due to *in situ* formation and not to scattered light, either from Herbig-Haro objects or from nearby H II regions. The relatively great strength of the red [S II] lines indicates an "HH object–like" spectrum. The attempt to understand the origin of this spectrum poses intriguing problems. It is present in a rather wide area surrounding HH 1 and HH 2 (extending at least as far as our observations go, i.e., out to a distance of approximately 1′). We do believe that HH spectra are generated behind shock waves. So, which are the shock waves responsible for this diffuse emission-line formation? We do not yet know the answer to this question. A possible speculative answer could be that this is the "remnant radiation" of the shock waves which went through the region earlier and that the emission is still going on because the recombination times are very long for $N_e \lesssim 10^2$ cm^{-3}. It is, however, worth noting that presently the lines are very narrow compared with those in HH objects. It is also intriguing that the line emission is not restricted to narrow "jets" originating from the C-S star (as one might have expected).

It would, of course, be highly interesting to determine the spatial distribution of the line emission in the whole environment of HH 1 and HH 2. As stated above, the line intensities vary only slightly with the position of the slit. It is not possible to make very detailed statements at the present time. This background radiation is sufficiently weak that considerable sampling is always required in order to improve the signal-to-noise ratio.

We are grateful to the staff of the Calar Alto and to Dr. H. Ulrich for their assistance during the observations. We would also like to thank Drs. U. Carsenty and H. Ulrich for their help concerning the data reductions. One of us (K. H. B.) has profited from discussions of the bow shock problems with Dr. S. U. Choe (University of Minnesota) and Mr. Alex Raga (University of Washington). We are grateful to Dr. G. H. Herbig for making available to us the photograph on which Figure 1 is based.

K. H. B's research has been supported by NSF grant AST 8314551 to the University of Washington.

REFERENCES

Böhm, K.-H. 1983, *Rev. Mexicana Astr. Ap.*, **7**, 55.
Böhm, K.-H., Böhm-Vitense, E., and Brugel, E. 1981, *Ap. J. (Letters)*, **245**, L113.
Böhm, K.-H., Siegmund, W. A., and Schwartz, R. D. 1976, *Ap. J.*, **203**, 399.
Böhm-Vitense, E., Böhm, K.-H., Cardelli, J. A., and Nemec, J. M. 1982, *Ap. J.*, **262**, 224.
Brugel, E. W., Böhm, K.-H., and Mannery, E. 1981, *Ap. J., Suppl.*, **47**, 117.
Brugel, E. W., Böhm, K.-H., Shull, J. M., and Böhm-Vitense, E. 1985, *Ap. J. (Letters)*, submitted.
Brugel, E. W., Shull, J. M., and Seab, C. G. 1982, *Ap. J. (Letters)*, **262**, L35.
Choe, S.-U. 1984, Ph.D. thesis, University of Minnesota.
Choe, S.-U., Böhm, K.-H., and Solf, J. 1985, *Ap. J.*, **288**, 338.

Cohen, M., and Schwartz, R. D. 1979, *Ap. J.* (*Letters*), **233**, L77.
Goudis, C. 1982, *The Orion Complex: A Case Study of Interstellar Matter* (Dordrecht: Reidel), pp. 45–47.
Hartmann, L., and Raymond, J. C. 1984, *Ap. J.*, **276**, 560.
Herbig, G. H. 1974, *Lick Obs. Bull.*, No. 658.
Herbig, G. H., and Jones, B. F. 1981, *A.J.*, **86**, 1232.
Koeppen, J., 1983, private communication.
Mundt, R., and Hartmann, L. 1983, *Ap. J.*, **268**, 766.
Norman, C. A., and Silk, J. 1979, *Ap. J.*, **228**, 197.
Ortolani, S., and D'Odorico, S. 1980, *Astr. Ap.*, **83**, L8.
Osterbrock, D. E. 1974, *Astrophysics of Gaseous Nebulae* (San Francisco: Freeman).
Pradhan, A. M. 1978, *M.N.R.A.S.*, **183**, 89P.
Raga, A., and Böhm, K.-H. 1985, *Ap. J. Suppl.*, **58**, 201.
Schwartz, R. D. 1975, *Ap. J.*, **195**, 631.
———. 1978, *Ap. J.*, **223**, 884.
———. 1981, *Ap. J.*, **243**, 197.
———. 1983*a*, *Ap. J.* (*Letters*), **268**, L37.
———. 1983*b*, *Rev. Mexicana Astr. Ap.*, **7**, 27.
Schwartz, R. D., and Dopita, M. A. 1980, *Ap. J.*, **236**, 543.
Solf, J., and Carsenty, U. 1982, *Astr. Ap.*, **113**, 142.
Trefzger, Ch., and Solf, J. 1978, *Astr. Ap.*, **63**, 131.

K.-H. Böhm: Department of Astronomy, University of Washington, Seattle, WA 98195

J. Solf: Max-Planck-Institut für Astronomie, Königstuhl, D-6900 Heidelberg 1, FRG